# Evolution of the Global Internal Dynamics of a Living Cell Nucleus during Interphase

M. Suissa,[†] C. Place,[†‡] E. Goillot,[§] and E. Freyssingeas[†*]

[†]Université de Lyon, Laboratoire de Physique, CNRS UMR 5672, École Normale Supérieure de Lyon, 69364 Lyon, France; [‡]Université de Lyon, Laboratoire transdisciplinaire Joliot-Curie, CNRS USR 3010, École Normale Supérieure de Lyon, 69364 Lyon, France; and [§]Université de Lyon, Laboratoire de Biologie Moléculaire de la cellule, CNRS UMR 5239, École Normale Supérieure de Lyon, CNRS, 69364 Lyon, France

ABSTRACT   Progress in cellular biology based on fluorescent microscopy techniques, shows that the spatial organization of the nucleus is dynamic. This dynamic is very complex and involves a multitude of phenomena that occur on very different time and size scales. Using an original light scattering experimental device, we investigated the global internal dynamics of the nucleus of a living cell according to the phases of the cell cycle. This dynamic presents two different and independent kinds of relaxation that are well separated in time and specific to the phase of the cell cycle.

## INTRODUCTION

Progress in cellular biology has indicated that the spatial organization of the nucleus is dynamic (1–8). A large number of experiments have been carried out to investigate this dynamic using fluorescent microscopy techniques (9–15). All of these investigations have produced a set of results, which show that the internal dynamics of the nucleus is very complex and includes many different processes, occurring on very different time and size scales. These studies suggest that this dynamic is a function of the biological activity of the nucleus. However, all previous studies only provide partial information on the nucleus dynamics as they only show the dynamics of processes associated with biological objects that are labeled. Hence, there is no information on correlations between different processes, and as a consequence the global internal dynamics of the nucleus remains poorly known. Yet, it is obvious that detailed knowledge of the global dynamics would be very useful to complete the current picture we have of the living cell nucleus.

In previous work (16,17), we showed that the global internal dynamics of a living cell nucleus could be probed by means of quasi elastic light scattering (QELS) experiments. Using an original QELS set-up we investigated this dynamic in the case of nuclei of living cells treated with a DNA replication inhibitor (hydroxyurea [HU]). We observed that the internal dynamics of the nucleus exhibits many relaxation times, from millisecond to a few dozen of seconds and is heterogeneous, both in time and space. In this study we report on the internal dynamics of a living cell nucleus during the different phases of the cell cycle by means of QELS experiments. Our results show that the internal dynamics of a living cell nucleus evolves as the cell progresses through the cell cycle. In particular, we are able to observe two independent kinds of relaxation, which we

have investigated in detail. The slowest relaxation time has a characteristic time $\tau_2$ of the order of 1 s and probably originates from the Brownian diffusion of large protein clusters through the nucleus. The fastest relaxation time seems to be due to very broad distributions of processes, most probably associated with chromatin remodeling. This relaxation time is smaller and its distribution broader as the chromatin evolves from a condensed state (early G1-phase) to the most uncondensed state (S-phase).

## MATERIALS AND METHODS

### QELS measurements and experimental set-up

QELS is a well-known technique in physics (18,19) that provides information on the global dynamics of the investigated system. QELS is particularly useful to investigate processes that are correlated both in time and space. The principle of QELS is to record and analyze the time fluctuations of the light intensity scattered by the sample. In practice, a laser beam passes through the sample and, in a given direction $\theta$ (i.e., for a given scattering wave vector **q**), the scattered light intensity $I(\mathbf{q},t)$ is detected with a photo-detector. Because light Scattering processes arise from local fluctuations of the sample refractive index: $\delta n(\mathbf{r},t)$ (18), QELS experiments lead to information on the dynamics of processes such as fluctuations of density, concentration, local "organization", and chemical composition.

In the case of the nucleus, the scattering volume is made up of both chromosome territories and an interchromosome domain. Inside these territories there are both motions (20,21) and remodeling (7,20–25) of chromatin fibers. In the interchromosome domain displacements and changes of the various nuclear body structures (13,24,25), diffusion of macromolecular "complexes" (such as protein clusters) as well as diffusion of small molecules (proteins, nucleotides…) (2,6,11,12,26–28) are observed. All these processes induce local variations in the nucleus refractive index and therefore scatter light.

Information on the nucleus internal dynamics can be obtained by measuring the time autocorrelation functions of the scattered intensity, namely $+I(0)I(t)$,. This function compares the scattered light intensity with itself at two different times; 0 and $t$ and the decay of this function as a function of $t$ (i.e., the autocorrelation loss), gives rise to the sample dynamics. As a consequence, we expect to observe many different mechanisms, hence many relaxation times. As we already observed (16,17), the recorded autocorrelation functions are bimodal and they do not reach a base line (Fig. 1). This latter feature arises from the existence of relaxation
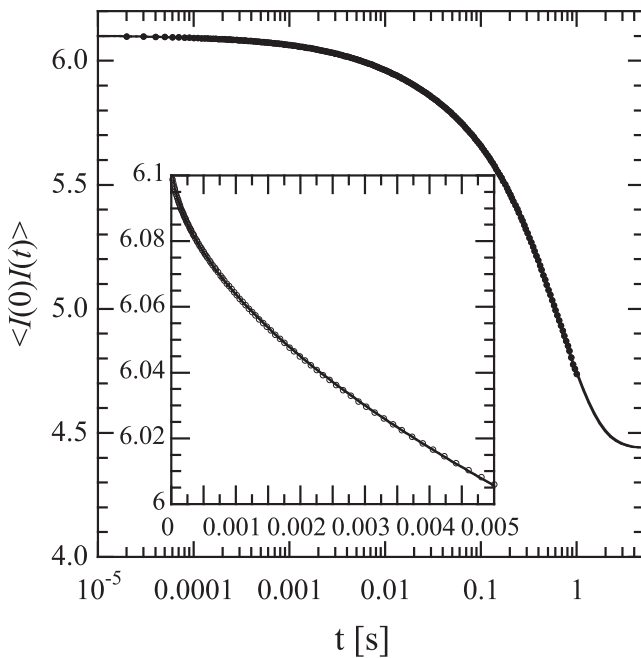
doi: 10.1016/j.bpj.2009.04.046

FIGURE 1 Typical autocorrelation function recorded from QELS experiment on a nucleus ($\phi \approx 34°$) on semilog scale. The solid line is the curve fit obtained using the equation provided in the text. (*Inset*) Very short times of the autocorrelation function (delay times $< 5 \times 10^{-3}$ s) in linear sale; the solid line is the curve fit obtained using the test function: $A - Bt^{\alpha}$, this fit allows for the estimation of $\alpha$ (15).

times $>1$ s (16,17). The short time decay of these autocorrelation functions seems to be slower than that of an exponential (Fig. 1, *inset*). Due to this latter feature, the recorded autocorrelation functions are fitted to the following test function:

$$\langle I(0)I(t)\rangle = (A_1\exp(-(t/\tau 1)^{\alpha}) + A_2\exp(-t/\tau_2))^2 + B,$$

which always fits well the measured autocorrelation functions (Fig. 1). Because the autocorrelation functions are unknown for times $>1$ s, the fitting process has to be carried out with care (17). Numerical simulations showed that using this procedure the values of $\tau_1$ and $\alpha$ are rather well estimated, the discrepancy for the value of $\tau_2$, however, is much larger (17).

The experimental set-up we used is described in detail in Suissa et al. (17). The beam of a He-Ne laser ($\lambda = 632.8$ nm, power in the range 0.1—0.5 mW) is focused with a microscope objective onto a glass surface on which the cells are adherent. This objective lens is also used to visualize, with a CCD camera (Kappa DX2H; Kappa Opto-Electronics GmbH, Gleinchen, Germany; monitored by LYNX; Clara Vision, Massy, France), a field of this surface of ~150 × 150 $\mu m^2$. This setup allows us to see the cells on the surface as well as the reflection from the laser beam. Then the nucleus of one cell is brought into contact with the laser beam. In a given direction we form the image of the illuminated volume of the nucleus on the entrance face of a monomodal optical fiber (the scattering volume is estimated to be of ~50 $\mu m^3$). The detected light is time correlated using a correlator (Brookhaven BI-9000; Brookhaven Instruments, Holtsville, NY). This correlator builds the autocorrelation function of the scattered intensity, for times included between $10^{-5}$ and a few seconds, allowing us to probe the sample dynamics in the range of $10^{-4}$–1 s. The polarization of the incoming beam is parallel to the scattering plane and there is no analyzer placed before the detector, therefore all the polarizations are measured. Transmission measurements through the nucleus showed that $>95\%$ of the incoming intensity is transmitted. We can thus conclude that the scattering is weak and therefore

multiple scattering can be neglected. Note that for all the experiments described here, the direction of the detector with the incoming beam made an angle $\phi$ of $34° \pm 1°$ that corresponds to a scattering angle $\theta$ of ~$24° \pm 2°$ (17).

## Experimental system

Our aim was to investigate the evolution of the internal dynamics of the cell nucleus in the different phases of the cell cycle. We carried out this study using a neuroblastoma cell line called SHEP. These cells are tumor cells of neural origin (29). (See details about cell culture conditions and protocol in the Supporting Material Part A and Suissa et al. (17).) Under normal culture conditions, SHEP cells have the following repartition: ~60%, 15%, and 25% of cells in G1-, S-, and G2/M-phase, respectively. As a simple visual observation does not allow distinguishing the different phases of the cell cycle, the measured distributions obtained on such populations, D(Natur.), are blends that reflect this particular cell repartition, i.e., $D(Natur.) \approx 0.6D(G1) + 0.15D(S) + 0.25D(G2)$, where $D(G1)$, $D(S)$, and $D(G2)$ are the distributions of pure G1-, S-, and G2-phases, respectively. Using a cytostatic drug, HU (30,31), cell populations can be synchronized. This procedure allows us to work with three different kinds of cell populations: 1), a population of cells in which cells in G1-phase are dominant; 2), a population of cells in which cells in S-phase are dominant; and 3), a population of cells in which cells in G2-phase are dominant. By combining these three different distributions we can obtain the respective distributions of the pure G1-, S-, and G2-phases.

First, SHEP cells are left at 37°C in a culture medium containing 0.5 mM of HU for 15 hr (see the Supporting Material Part A). Then, cell cultures are released from HU by removing medium containing HU. After such a treatment, we notice that the evolution of the cell populations displays three different time periods that we call: G1*, S*, and G2* periods, during which the G1-, S-, and G2-phases are dominant, successively (Fig. 2) (see details in the Supporting Material Part A). In the G1* period, ~90%, 5%, and 5% of the cell populations are in the G1-, S-, and G2-phases, respectively. For
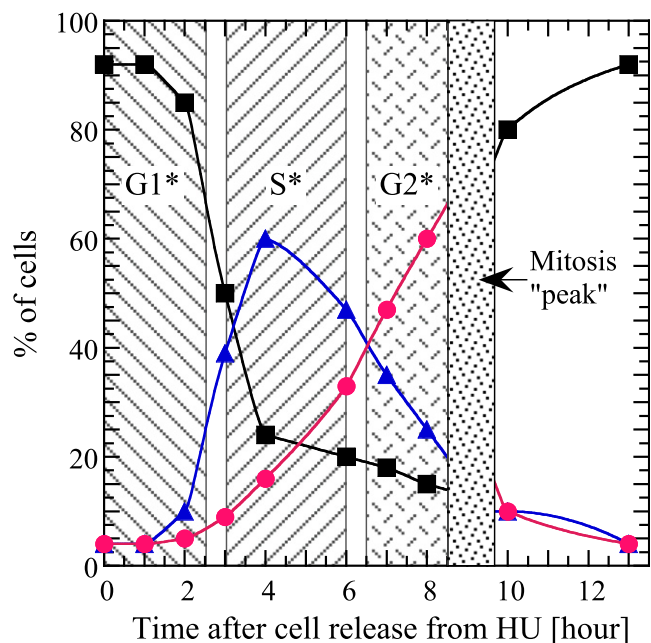


FIGURE 2 Cell distribution over the different phases, G1 (*squares*), S (*triangles*), and G2/M (*circles*) respectively, as a function of time after replacing the culture medium containing 0.5 mM of HU by the usual culture medium (color online; *black*: G1-phase, *blue*: S-phase, *red*: G2-phase). (Results obtained by fluorescence activated cell sorter analysis; see details in the Supporting Material Part A).

the S* period, ~50%, 25%, and 25% of the investigated cells are in S-, G1-, and G2-phases, respectively. Finally the G2* period contains ~55%, 25%, and 20% of the investigated cells in G2-, S-, and G1-phases, respectively. For each period, the obtained distributions should reflect the cell repartition. Therefore the measured distributions during the G1*, S*, and G2* periods, i.e., $D(G1^*)$, $D(S^*)$, and $D(G2^*)$, respectively, are linked to the distributions of the pure phases, $D(G1)$, $D(S)$, and $D(G2)$ by the following relations: $D(G1^*) \approx 0.9D(G1) + 0.05D(S) + 0.05D(G2)$; $D(S^*) \approx 0.25D(G1) + 0.55D(S) + 0.2D(G2)$; and $D(G2^*) \approx 0.2D(G1) + 0.25D(S) + 0.55D(G2)$. Hence, we can deduce estimations of $D(G1)$, $D(S)$, and $D(G2)$ that are simply given by Eqs. 1–3, respectively:

$$D(G1) \approx (86D(G1^*) - 5D(S^*) - 6D(G2^*))/75, \quad (1)$$

$$D(S) \approx (-20D(G1^*) + 99D(S^*) - 34D(G2^*))/45, \quad (2)$$

$$D(G2) \approx (-8D(G1^*) - 36D(S^*) + 81D(G2^*))/37. \quad (3)$$

The characteristics of the different experiments that were carried out for investigating the G1*, S*, and G2* periods are indicated in the Supporting Material Part A. For each investigated period, the measurements taken on the different cell cultures always give the same features for the respective distributions of $\tau_1$, $\alpha$, and $\tau_2$, indicating that the obtained results are reproducible.

## RESULTS AND DISCUSSION

As we observed previously (16,17), the time $\tau_2$ is always at least one order of magnitude larger than the characteristic time $\tau_1$. We never observe any functional relationship between both timescales; $\tau_1$ and $\tau_2$ always seem to be independent from one to another. Therefore we believe these two relaxations correspond to independent biological processes. Furthermore, no correspondence between the values of $\alpha$ and $\tau_1$ is ever found.

## Measurements analysis

The complexity of the system composition and the large number of relaxation mechanisms that this complexity implies is not the only difficulty, which is met when investigating the nucleus dynamics. Both composition and structure of the nucleus are not spatially homogenous (32). The nucleus is an active system with chemical reactions taking place continuously. It is a system that slowly evolves with time as the cell cycle progresses (for example, the amount of DNA is doubled during the S-phase). Very different activities can simultaneously occur at a very short distance from one another. (Indeed, at a given time, two completely different activities can occur in two neighboring chromosome territories, for example, at the same time in the nucleus, there are always both transcription and repair activities as well as other activities in the different nuclear foci (33–35).) The activity within a given chromosome territory can vary over rather short time periods (33–35). Hence, because the scattering volume is smaller than the nucleus volume (the scattering volume has a size of ~50 $\mu m^3$ and contains ~8 chromosome territories), one expects the probed dynamics to depend on its location. One also expects the probed

dynamics to vary as a function of time due to displacements and reorientations of the chromosome territories as well as activity variations within the chromosome territories. Therefore, the measurement of only one single autocorrelation function of the scattered intensity cannot give access to the overall internal dynamics of the nucleus, but only a "snapshot" of this dynamic, in the scattering volume. Indeed, for each investigated nucleus, we observe large variations in the measured values of $\tau_1$, $\tau_2$, and $\alpha$ from one measurement to another. However, by repeating these measurements many times on the same "system" (i.e., different nuclei and so different scattering volumes, and on cells in the same cell cycle phase), characteristic time distributions reflecting the global internal dynamics of the nucleus during this particular stage can be obtained. To observe the changes in the internal dynamics of the nucleus as a function of the phases of the cell cycle, we simply compare the probability densities of these three parameters following the procedure we used in Suissa et al. (17). This particular data analysis allows for the investigation of multimodal distributions because the width of the measurement is taken into account.

## Slow dynamics

### Evolution of the slow dynamics during interphase

The probability densities obtained for $\tau_2$ times during the G1*, S*, and G2* periods are displayed in Fig. 3 a. For the G1* period the distribution exhibits a broad and asymmetrical bump, with a long tail, whose maximum is located at ~0.5 s. In the S* period the measured distribution still presents a broad and asymmetrical bump, with a long tail, whose maximum is now located at ~0.62 s. For the G2* period the probability density of $\tau_2$ times again displays a broad and asymmetrical bump, whose maximum is located around 0.85 s.

Using these distributions and Eqs. 1–3, the probability densities of $\tau_2$ times for pure G1-, S-, and G2-phases have been estimated and are presented in Fig. 3 b. Distributions of $\tau_2$ times in the G1- and S-phases do not seem very different even if the distribution in the S-phase seems to be slightly broader. In the G2-phase, we observe an important shift to slower times for the slow dynamics. Our results show clearly a diminished rate in the internal slow dynamics of the nucleus as the cell cycle progresses. We note that diminishing times of these slow dynamics within the nucleus was observed in presence of HU in the cell culture medium for cells in S- or G2-phases with regard to cells in G1-phase (17).

### Interpretation

We have shown previously (16) that this slow dynamic is very likely diffusive in nature, with a mean diffusion coefficient $D$ of the order of $4.10^{-2}$ $\mu m^2 s^{-1}$. This value of the mean diffusion coefficient is very similar to those obtained by Shav-Tal et al. (11) for the diffusion of mRNA–proteins complexes within the nucleus ($10^{-2}$–$9.10^{-2}$ $\mu m^2 s^{-1}$). Therefore we believe that this slow relaxation originates from the
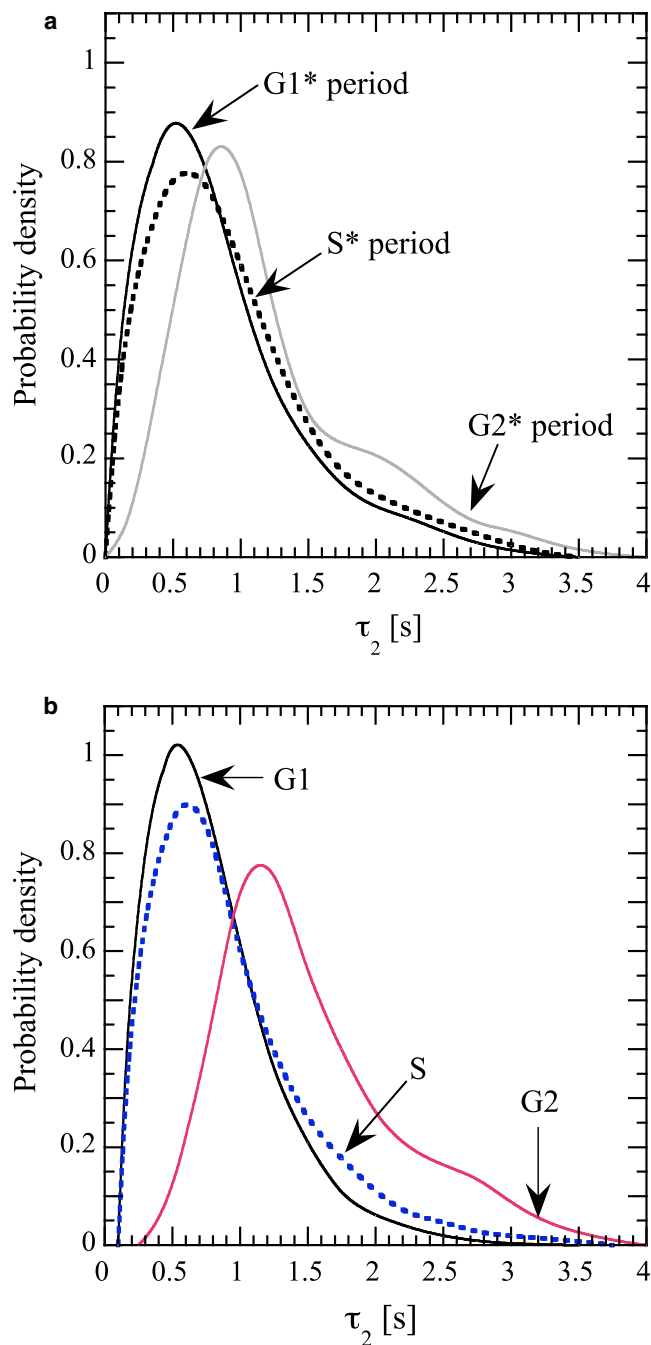
FIGURE 3 (*a*) Measured probability densities of $\tau_2$ times obtained: during the G1* period, the S* period, and the G2* period, respectively. (*b*) Probability densities of the relaxation time $\tau_2$ estimated from the raw results by using Eqs. 1–3 (color online; *black line*: G1-phase, *blue line*: S-phase, *red line*: G2-phase).

Brownian diffusion of large ''objects'', such as mRNA–proteins complexes or transcription machinery within the nucleus. In that case, the observed slowdown as the cell cycle progresses may be explained by an increase in the nucleus viscosity due to the increase in its concentration after DNA replication. We notice that the slow dynamics is about twice as slow in the G2-phase than in the G1-phase. This result

suggests that the diffusion of these ''objects'' through the nucleus is likely diffusion hindered by fixed obstacles that must be bypassed (a 3D labyrinth), rather than diffusion through an entanglement such as that seen in the case of a concentrated polymer solutions. Otherwise, the effect of the increase of the concentration on the viscosity would be much stronger. Furthermore, in the framework of a Brownian motion of large ''objects,'' this particular relaxation time is related to the mean size of the objects present in the scattering volume, assuming they all experience the same viscosity. Because there is only a small number of these ''objects'' in the scattering volume, one can imagine that the variations in the measured values of $\tau_2$ convey the time fluctuations of the size distribution of these large ''objects'' within the scattering volume. Hence, the distributions of $\tau_2$ times likely reproduce the size distributions of these large ''objects'' inside the nucleus.

## Fast dynamics

### Evolution of the fast dynamics during interphase

*G1* period*. The measured probability density of $\tau_1$ times for this period is broad and exhibits two maxima: around 22 and 35 ms, respectively (Fig. 4 *a*) whereas the probability density of $\alpha$ shows a broad asymmetrical maximum located around 0.68 (Fig. 4 *a*, *inset*).

*S* period*. The probability density of the $\tau_1$ times has an asymmetrical shoulder whose maximum is located around 15 ms (Fig. 4 *b*). It is noticeably different from that obtained in the G1* period. On the other hand, the distribution of the stretching coefficient $\alpha$ is not that different from that of the G1* period. The probability density of $\alpha$ shows a maximum located around 0.62 (Fig. 4 *b*, *inset*).

*G2* period*. This period displays a probability density of $\tau_1$ times whose maximum is located around 20 ms (Fig. 4 *c*), hence different from that obtained in the G1* period but rather similar to that obtained in the S* period and the stretching coefficient $\alpha$ exhibits a maximum located around 0.75 (Fig. 4 *c*, *inset*). It is therefore very different from those obtained in both other periods.

It should be noticed that the G1* period shows clearly two distinct kinds of nuclei having different fast dynamics. Indeed we observe that 11 nuclei of 24, i.e., 46% of the investigated nuclei, contribute to the peak at 22 ms only, whereas the other nuclei contribute to the second peak. Note that this bimodal distribution of nuclei was already observed for nuclei of SHEP cells in G1-phase in a culture medium containing HU (16). For both kinds of nuclei the distributions of $\alpha$ seem similar.

Using these raw distributions and Eqs. 1–3, the probability densities of $\tau_1$ times and $\alpha$ for pure G1-, S- and G2-phases can be estimated and are displayed in Fig. 5, *a* and *b*, for $\tau_1$ times and $\alpha$, respectively. The differences observed show the strong modifications occurring to the fast internal dynamics of a living cell nucleus when the cell cycle progresses.
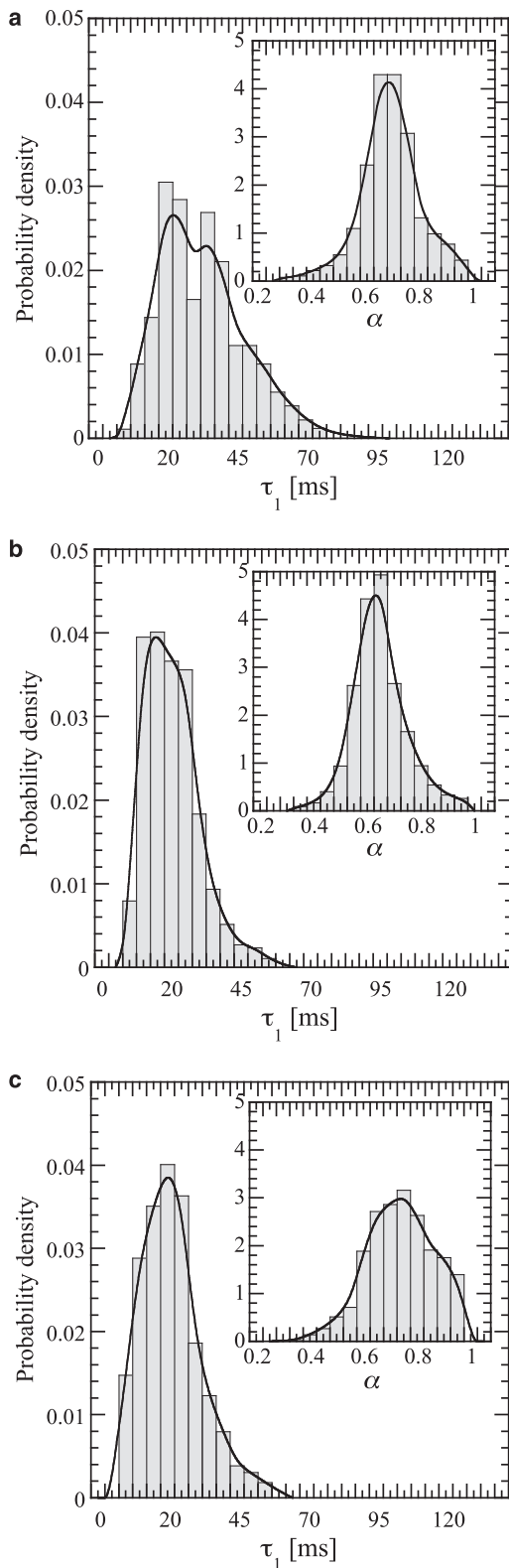
FIGURE 4   Probability density of $\tau_1$ times obtained during the (*a*) G1*, (*b*) S*, and (*c*) G2* periods, respectively. (*Inset*) Corresponding probability density of the stretching coefficient $\alpha$.
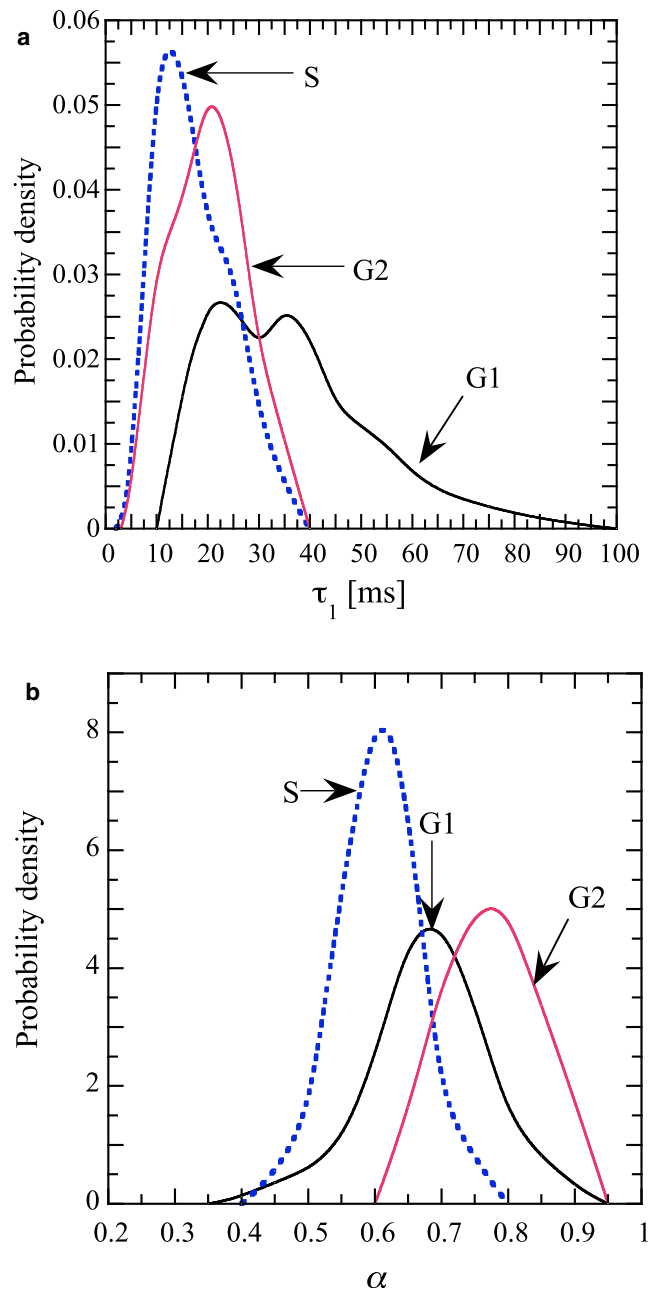


FIGURE 5   (*a*) Probability densities of $\tau_1$ times estimated from the experimental results by using Eqs. 1–3. (*b*) Probability densities of $\alpha$ estimated the same way as those of $\tau_1$ and $\tau_2$ (color online; *black line*: G1-phase, *blue line*: S-phase, *red line*: G2-phase).

In the G1-phase, the probability density of $\tau_1$ times ranges from 10 to 90 ms and exhibits two maxima: around 22 and 35 ms, respectively. This distribution is indeed the sum of two independent distributions. One, rather narrow, ranging from 10 to 40 ms and whose maximum is located at ~22 ms and a second, which is much broader, that ranges from 30 to 90 ms and whose maximum is located around 40 ms (see the Supporting Material Part B). The probability density of

$\alpha$ shows a broad and asymmetrical shoulder with a maximum located around 0.68.

For the S-phase, the probability density of $\tau_1$ times is less broad; and ranges from 5 to 35 ms with one maximum at ~10 ms and one shoulder around 25 ms. In contrast to this the probability density of $\alpha$ presents a high and narrow peak located around 0.62.

Finally the $\tau_1$ time probability density of the G2-phase ranges from 5 to 40 ms and shows a shoulder around 10 ms with a maximum around 20 ms. The probability density of $\alpha$ is much broader, and exhibits a maximum at ~0.75–0.8.

### Interpretation

The fast part of the autocorrelation functions decreases as a function of time with a stretched-exponential decay. A wide variety of relaxation behavior can be fitted with such a function. A commonly used interpretation is in terms of the global relaxation of a system having a set of relaxation processes, each of which decays exponentially in time with a specific characteristic time (36,37). The characteristic time provided by the fit with this kind of function is somehow related to the average over all the characteristic times of the distribution. The value of the stretching coefficient, which defines the deviation from a single exponential decay, is related to the width of the distribution of relaxation times; the distribution being all the more broad because $\alpha$ is small compare to 1. (According to the numerical simulations we carried out, for a time distribution $P(\tau)$ given by a log-normal law, i.e., $P(\tau) = \exp(-(\ln(\tau/\mu))^2/2\sigma^2)/(\tau\sigma\sqrt{2\pi})$, we find a stretched exponential decay of the autocorrelation function, i.e., $\exp(-(t/\tau_1)^\alpha)$, where: $\tau_1 \approx \mu(1 + a\sigma^2)$ and $\alpha \approx 1/(1 + \sigma^2)^b$, with $a \approx 0.11$ and $b \approx 0.5$.). Hence, to understand this complex dynamic one has to focus on both $\tau_1$ and $\alpha$ at the same time and not on each of them independently. In this study, at least in the G1- and S-phases, most of the measured values of $\alpha$ are $<0.7$. Such values of $\alpha$ indicate that the probed distributions of relaxation times contributing to the fast dynamics are very broad. According to numerical simulations we carried out, we believe that such low values of $\alpha$ very likely indicate that the probed distributions of relaxation times are log-normal distributions, or sums of log-normal distributions that overlap. According to Castaing and Souletie (39), log-normal distributions of relaxation times originate from the existence of hierarchical processes monitoring the time evolution from one level to the following (i.e., similar to ageing processes (39–42)).

Assuming log-normal distributions of relaxation times, for each phase of the cell cycle, we can estimate the most probable distributions of relaxation times contributing to the fast dynamics that are probed during QELS experiments. These distributions are estimated using the most probable values of both $\tau_1$ and $\alpha$ for each phase. (Table 1). We display these estimated time distributions in Fig. 6 and observe that they are very different from one phase to another.

**TABLE 1 For each phase of the cell cycle, values of both $\tau_1$ and $\alpha$ used to estimate the most probable time distributions displayed in Fig. 6**

| Phase of the cell cycle | $\tau_1$ (ms) | $\alpha$ |
|---|---|---|
| "Fast" G1 | 22 | 0.69 |
| "Slow" G1 | 40 | 0.69 |
| S | 10 | 0.61 |
| G2 | 20 | 0.79 |

In the G1-phase (for both fast and slow nuclei), according to the estimated distributions of relaxation times, the fast dynamics seems to be characterized by a strong contribution of the slow relaxations, i.e., with relaxation times larger than typically a few $10^{-2}$ s. This contribution is more important than in the S- and G2-phases. The weight of the processes having relaxation times $>4.10^{-2}$ s in these time distributions is of ~25% and 40% for the "fast" and the "slow" G1-phase, respectively, whereas it is $<15\%$ for both the S- and G2-phases.

The estimated distribution of relaxation for the S-phase, times is characterized by an important weight of the fast relaxation times, i.e., with relaxation times typically $>10^{-2}$ s. This contribution is much larger in this case than in the other phases; ~50% of the distribution in the S-phase and $<25\%$ in the other. Hence, in relation to the fast dynamics in the other phases, the fast dynamics in the S-phase likely involves much faster processes.

In the G2-phase, the estimated distribution of relaxation times seems to range over only 2 decades; from $10^{-3}$ to 0.1 s. Therefore, the fast dynamics in the G2-phase is likely to be less rich and complex than those in G1- or S-phases.

At this stage of our investigation, we have no clear connections between our measurements and biological processes. However, chromatin is the main compound of the scattering volume and chromatin structure is known to be hierarchical (43–45). Therefore we conjecture that the remodeling of chromatin fibers is carried out by an ordered succession of different processes, each process having its own characteristic time. It is also known that the chromatin compaction evolves during the cell cycle (46); chromatin is highly condensed at the beginning of the G1-phase and decondensed continually as the cell progresses through the G1- and S-phases. It will condense again at the very end of the G2-phase, just before mitosis. We can imagine that the more compact the chromatin is, the more complex and hierarchical the compaction must be. This inevitably must lead to the appearance of processes with long characteristic times in the remodeling dynamics. The strong chromatin compaction in the early G1-phase might explain why in this phase we observe slower processes than in both other phases where chromatin compaction is less. Furthermore,
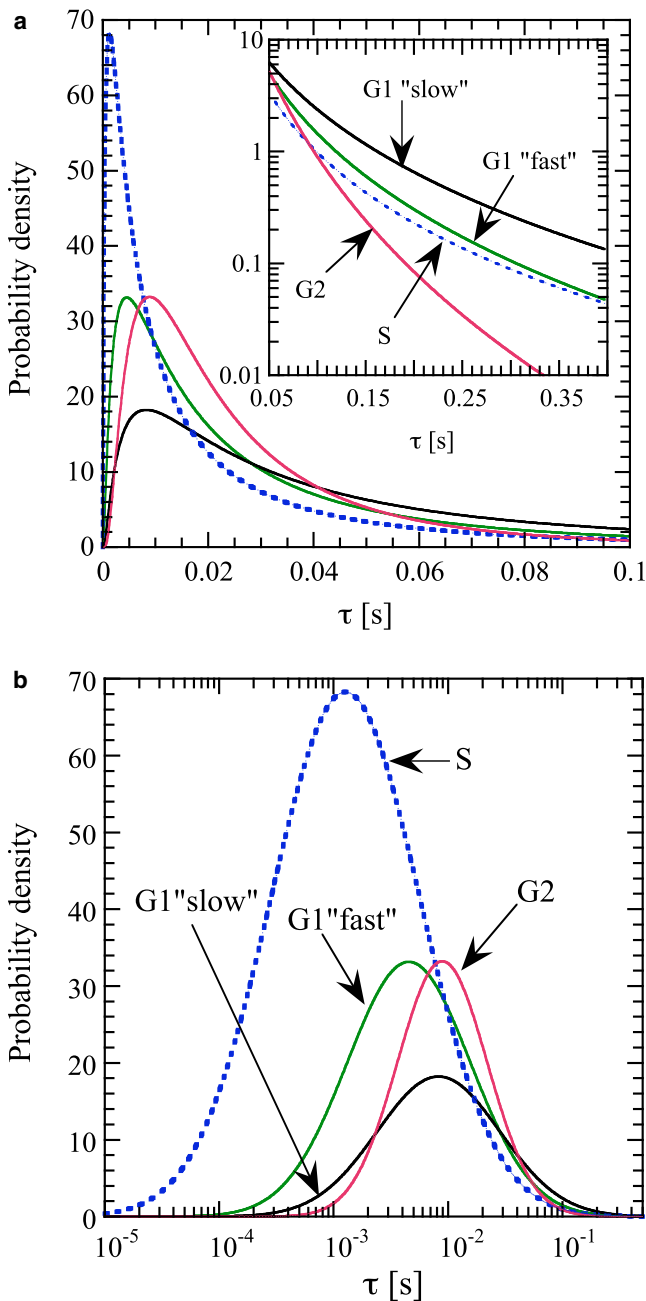
FIGURE 6 (*a*) Most probable distributions of relaxation times contributing to the fast mode for every phase of the cell cycle on a linear scale (color online; *green*: "fast" G1-phase, *black*: "slow" G1-phase, *blue*: S-phase; *red*: G2-phase). (*Inset*) Enlargement of these distributions at "long" times on a semilog scale (i.e., $\tau \geq 5 \times 10^{-2}$ s). (*b*) Most probable distributions of relaxation times contributing to the fast mode for every phase of the cell cycle on a semilog scale (same colors).

one can speculate that the chromatin restructuring processes are likely to be faster as well as much more complex in the S-phase, where replication takes place and lasts for 2 h, in contrast to the G1-phase, which lasts for ~10 h and where the main activity within the nuclei is transcription, or the G2-phase. As a consequence, in Suissa et al. (16,17), we made the hypothesis that this fast mode might originate from

chromatin remodeling. This hypothesis also seems consistent with the fact that in the G1-phase the distributions of relaxation times seem to be much less broad for cells grown in a normal culture medium than for cells treated with HU, which inhibits DNA replication (16,17) (Supporting Material Part C). Indeed, HU induces histones phosphorylation and foci formation of H2AX (47) that should cause a different chromatin compaction and therefore different remodeling processes. Following this hypothesis, one can propose that both dynamics observed in the G1-phase reflect the existence of two different states of chromatin compaction during this phase. These different states may be within the nucleus itself, with both chromatin states: euchromatin and heterochromatin. The chromatin compaction for these two states is, indeed, different and different dynamics can be expected depending on whether we probe euchromatin or heterochromatin. However, these two dynamics might also originate from different chromatin compactions at different stages of the G1-phase (46); i.e., a different chromatin compaction whether the cell is at the beginning or the end of the G1-phase.

To test out this hypothesis several experiments could be carried out. For example, one can think of carrying out QELS experiments on nuclei for which the remodeling of chromatin has been modified by using ATP depletion (23,24), chromatin ATP-dependent remodelers such as SWI/SNF (48), heat shock (49), or virus infection of the cells (50).

## CONCLUSIONS

To our knowledge, this work is one of the first attempts to investigate the global internal dynamics of the living cell nucleus. This study was carried by means of dynamic light scattering experiments, using an experimental device we specially built for that purpose. The internal dynamics of the nucleus is probed in the timescale from milliseconds up to times of the order of 1 s by measuring the autocorrelation function of the scattered light intensity. Over this time range, the autocorrelation functions of the scattered intensity are bimodal, clearly demonstrating the existence of two different relaxations well separated in time. Our measurements give access to three parameters; two characterizing the fast dynamics: the time $\tau_1$ and the stretching coefficient $\alpha$, and one characterizing the slow dynamics the time, $\tau_2$. In this study, we present an investigation of this dynamic in the different phases of the interphase; G1-, S-, and G2-phases of the cell cycle. Results indicate clearly that the nucleus internal dynamics evolves according to the phase of the cell cycle.

1. For each investigated nucleus we observe large variations in the measured values of $\tau_1$, $\tau_2$, and $\alpha$ from one measurement to another. This indicates that during our measurements we probe different mechanisms and observe several concomitant biological processes. Therefore, we can conclude that the internal dynamics of the living cell

nucleus is rich, complex and heterogeneous, both in time and space. This is not surprising because the nucleus is an active system with chemical reactions taking place continually. Furthermore, very different activities can simultaneously occur within the nucleus at very short distance from one another and, at a given time, two completely different activities can occur in two neighboring chromosome territories.

2. Because we do not find any functional relationship between them, we believe that both timescales we observe are completely independent from each other and therefore correspond to different biological processes having no link between them.

3. By repeating the measurements many times, on several different nuclei, we can build distributions for $\tau_1$, $\tau_2$, and $\alpha$ that give a picture of the internal dynamics of the living cell nucleus for times shorter than a few seconds. At this stage of our study, we have not yet found connections between our measurements and specific biological processes and thus, we cannot firmly assign the different characteristic times we observe to a particular biological phenomenon, or a mix of different biological phenomena. Nevertheless, we can put forward some hypotheses concerning the different timescales.

The slowest relaxation has a characteristic time $\tau_2$ of the order of 0.5–1 s and we believe that this slow relaxation originates from the Brownian diffusion of large protein clusters through the nucleus. Therefore, the observed slowdown of this slow relaxation in the S- and mainly in the G2-phase in comparison to the G1-phase might be explained by an increase in the nucleus viscosity due to the increase in its concentration.

The fastest relaxation seems to be due to a set of processes leading to a very broad continuous distribution of characteristic times. Our results show that in any sub volume of the nucleus larger than a few chromosome territories, the distribution of processes at the origin of the fast dynamics continually evolves with time, likely according to the nucleus activity; the set of processes involved vary within a few minutes, some processes disappearing whereas others appear. Furthermore, for cells in the G1-phase, our results suggest the existence of two different kinds of fast dynamics. As this study is a pioneering investigation, it is difficult to draw definitive conclusions from the results. Nevertheless, we believe that the fast relaxation mode originates from the existence of hierarchical processes monitoring the time evolution from one level to the following. Hence, this fast relaxation might be due to a set of collective processes associated with the chromatin fibers remodeling.

4. Finally, we would like to insist on the fact that we believe that QELS experiments should prove useful for the study of the internal dynamics of living cell nuclei because this technique is likely to be complementary to fluorescence techniques, especially for investigating the chromatin

dynamics. Moreover, it seems that the analysis of the fast dynamics could be used to determine the phase of the cell cycle in which a cell is (see the Supporting Material Part D).

## SUPPORTING MATERIAL

Parts A–D, eight figures, and three tables are available at http://www.biophysj.org/biophysj/supplemental/S0006-3495(09)00952-7.

## REFERENCES

1. Pederson, T. 1999. Movement and localization of RNA in the cell nucleus. *FASEB J.* 13:S238–S242.

2. Gorski, S. A., M. Dundr, and T. Misteli. 2006. The road much traveled: trafficking in the cell nucleus. *Curr. Opin. Cell Biol.* 18:284–290.

3. Heun, P., T. Laroche, K. Shimada, P. Furrer, and S. M. Gasser. 2001. Chromosome dynamics in the yeast interphase nucleus. *Science.* 294:2181–2186.

4. Belmont, A. 2003. Dynamics of chromatin, proteins, and bodies within the cell nucleus. *Curr. Opin. Cell Biol.* 15:304–310.

5. Chubb, J. R., and W. A. Bickmore. 2003. Considering nuclear compartmentalization in the light of nuclear dynamics. *Cell.* 112:403–406.

6. Janicki, S. M., and D. L. Spector. 2003. Nuclear choreography: interpretations from living cells. *Curr. Opin. Cell Biol.* 15:149–157.

7. Ehrenhofer-Murray, A. E. 2004. Chromatin dynamics at DNA replication, transcription and repair. *Eur. J. Biochem.* 271:2335–2349.

8. Pederson, T. 2004. The spatial organization of the genome in mammalian cells. *Curr. Opin. Genet. Dev.* 14:203–209.

9. Shav-Tal, Y., X. Darzacq, and R. H. Singer. 2006. Gene expression within a dynamic nuclear landscape. *EMBO J.* 25:3469–3479.

10. Houtsmuller, A. B., and W. Vermeulen. 2001. Macromolecular dynamics in living cell nuclei revealed by fluorescence redistribution after photobleaching. *Histochem. Cell Biol.* 115:13–21.

11. Shav-Tal, Y., X. Darzacq, S. M. Shenoy, D. Fusco, S. M. Janicki, et al. 2004. Dynamics of single mRNPs in nuclei of living cells. *Science.* 304:1797–1800.

12. Beaudouin, J., F. Mora-Bermudez, T. Klee, N. Daigle, and J. Ellenberg. 2006. Dissecting the contribution of diffusion and interactions to the mobility of nuclear proteins. *Biophys. J.* 90:1878–1894.

13. Mora-Bermudez, F., and J. Ellenberg. 2007. Measuring structural dynamics of chromosomes in living cells by fluorescence microscopy. *Methods.* 41:158–167.

14. Wang, I. F., N. M. Reddy, and C. K. J. Shen. 2002. Higher order arrangement of the eukaryotic nuclear bodies. *Proc. Natl. Acad. Sci. USA.* 99:13583–13588.

15. Abney, J. R., B. Cutler, M. L. Fillbach, D. Axelrod, and B. A. Scalettar. 1997. Chromatin dynamics in interphase nuclei and its implications for nuclear structure. *J. Cell Biol.* 137:1459–1468.

16. Suissa, M., C. Place, E. Goillot, B. Berge, and E. Freyssingeas. 2007. Dynamic light scattering as an investigating tool to study the global internal dynamics of a living cell nucleus. *Europhys. Lett.* 78:38005.

17. Suissa, M., C. Place, E. Goillot, and E. Freyssingeas. 2008. Internal dynamics of a living cell nucleus investigated by dynamic light scattering. *Eur. Phys. J.E.* 26:435–448.

18. Berne, B. J., and R. Pecora. 2000. Dynamic Light Scattering: With Applications to Chemistry, Biology and Physics, 2nd ed. Dover Publications, Mineola, NY.

19. Brown, W. 1996. Light Scattering: Principles and Development (Monographs on the Physics and Chemistry of Materials). Clarendon Press, Oxford, UK.

20. Davis, S. K., and C. J. Bardeen. 2004. The connection between chromatin motion on the 100 nm length scale and core histone dynamics in live XTC-2 cells and isolated nuclei. *Biophys. J.* 86:555–564.

21. Levi, V., Q. Q. Ruan, M. Plutz, A. S. Belmont, and E. Gratton. 2005. Chromatin dynamics in interphase cells revealed by tracking in a two-photon excitation microscope. *Biophys. J.* 89:4275–4285.

22. Dundr, M., and T. Misteli. 2001. Functional architecture in the cell nucleus. *Biochem. J.* 356:297–310.

23. Mizuguchi, G., X. Shen, J. Landry, W. H. Wu, S. Sen, et al. 2004. ATP-driven exchange of histone H2AZ variant catalyzed by SWR1 chromatin remodeling complex. *Science.* 303:343–348.

24. Platani, M., I. Goldberg, A. I. Lamond, and J. R. Swedlow. 2002. Cajal body dynamics and association with chromatin are ATP-dependent. *Nat. Cell Biol.* 4:502–508.

25. Handwerger, K. E., and J. G. Gall. 2006. Subnuclear organelles: new insights into form and function. *Trends Cell Biol.* 16:19–26.

26. Phair, R. D., and T. Misteli. 2000. High mobility of proteins in the mammalian cell nucleus. *Nature.* 404:604–609.

27. Phair, R. D., P. Scaffidi, C. Elbi, J. Vecerova, A. Dey, et al. 2004. Global nature of dynamic protein-chromatin interactions in vivo: three-dimensional genome scanning and dynamic interaction networks of chromatin proteins. *Mol. Cell. Biol.* 24:6393–6402.

28. Politz, J. C., R. A. Tuft, and T. Pederson. 2003. Diffusion-based transport of nascent ribosomes in the nucleus. *Mol. Biol. Cell.* 14:4805–4812.

29. Johnsen, J. I., I. Pettersen, F. Ponthan, B. Sveinbjornsson, T. Flaegstad, et al. 2004. Synergistic induction of apoptosis in neuroblastoma cells using a combination of cytostatic drugs with interferon-gamma and Trail. *Int. J. Oncol.* 25:1849–1857.

30. Khayat, A. S., A. C. Guimaraes, P. C. Cardoso, P. D. L. de Lima, M. D. Bahia, et al. 2004. Mutagenicity of hydroxyurea in lymphocytes from patients with sickle cell disease. *Genet. Mol. Biol.* 27:115–117.

31. Koc, A., L. J. Wheeler, C. K. Mathews, and G. F. Merrill. 2004. Hydroxyurea arrests DNA replication by a mechanism that preserves basal dNTP pools. *J. Biol. Chem.* 279:223–230.

32. Banerjee, B., D. Bhattacharya, and G. V. Shivashankar. 2006. Chromatin structure exhibits spatio-temporal heterogeneity within the cell nucleus. *Biophys. J.* 91:2297–2303.

33. Zink, D., T. Cremer, R. Saffrich, R. Fischer, M. F. Trendelenburg, et al. 1998. Structure and dynamics of human interphase chromosome territories in vivo. *Hum. Genet.* 102:241–251.

34. Jong, A. Y., K. Yu, B. Zhou, T. Frgala, C. P. Reynolds, et al. 1998. A simple and sensitive ribonucleotide reductase assay. *J. Biomed. Sci.* 5:62–68.

35. Pombo, A., P. Cuello, W. Schul, J. B. Yoon, R. G. Roeder, et al. 1998. Regional and temporal specialization in the nucleus: a transcriptionally-active nuclear domain rich in PTF, Oct1 and PIKA antigens associates with specific chromosomes early in the cell cycle. *EMBO J.* 17:1768–1778.

36. Williams, G., and D. C. Watts. 1970. Nonsymmetrical dielectric relaxation behavior arising from a simple empirical decay function. *Trans. Faraday Soc.* 66:80–85.

37. Lindsey, C. P., and G. D. Patterson. 1980. Detailed comparison of the Williams-Watts and Cole-Davidson functions. *J. Chem. Phys.* 73:3348–3357.

38. Reference deleted in proof.

39. Castaing, B., and J. Souletie. 1991. Dynamics scaling and non-exponential relaxations in the presence of disorder. application to spin glasses. *J. Phys. I.* 1:403–414.

40. Bouchaud, J.-P. 1992. Weak ergodicity and aging in disordered systems. *J. Phys. I.* 2:1705–1713.

41. Bouchaud, J.-P., A. Comtet, and C. Monthus. 1995. On a dynamical model of glasses. *J. Phys. I.* 5:1521–1526.

42. Lubchenko, V., and P. G. Wolynes. 2004. Theory of aging in structural glasses. *J. Chem. Phys.* 121:2852–2865.

43. Belmont, A. S., and K. Bruce. 1994. Visualization of G1 chromosome: a folded, twisted, supercoiled chromonema model of interphase chromatid structure. *J. Cell Biol.* 127:287–302.

44. Kireeva, N., M. Lakonishok, I. Kireev, H. Tatsuya, and A. S. Belmont. 2004. Visualization of early chromosome condensation: a hierarchical folding, axial glue model of chromosome structure. *J. Cell Biol.* 166:775–785.

45. van Driel, R., P. F. Fransz, and P. J. Verschure. 2003. The eukaryotic genome: a system regulated at different hierarchical levels. *J. Cell Sci.* 116:4067–4075.

46. Kleckner, N., D. Zickler, G. H. Jones, J. Dekker, R. Padmore, et al. 2004. A mechanical basis for chromosome function. *Proc. Natl. Acad. Sci. USA.* 101:12592–12597.

47. Ward, I. M., and J. J. Chen. 2001. Histone H2AX is phosphorylated in an ATR-dependent manner in response to replicational stress. *J. Biol. Chem.* 276:47759–47762.

48. Peterson, C. L., and J. L. Workman. 2000. Promoter targeting and chromatin remodeling by the SWI/SNF complex. *Curr. Opin. Genet. Dev.* 10:187–192.

49. Kim, C., C. M. Rubin, and C. W. Schmid. 2001. Genome-wide chromatin remodeling modulates the Alu heat shock response. *Gene.* 276:127–133.

50. Lomonte, P., K. F. Sullivan, and R. D. Everett. 2001. Degradation of nucleosome-associated centromeric histone H3-like protein CENP-A induced by herpes simplex virus type 1 protein ICP0. *J. Biol. Chem.* 276:5829–5835.